Non-equilibrium quantum dynamics after local quenches

Uma Divakaran[1], Ferenc Iglói[2,3] and Heiko Rieger[1]

[1] Theoretische Physik, Universität des Saarlandes, D-66041 Saarbrücken, Germany
[2] Research Institute for Solid State Physics and Optics, PO Box 49, H-1525 Budapest, Hungary
[3] Institute of Theoretical Physics, Szeged University, H-6720 Szeged, Hungary
E-mail: uma.ker@gmail.com, igloi@szfki.hu and h.rieger@mx.uni-saarland.de

Abstract. We study the quantum dynamics resulting from preparing a one-dimensional quantum system in the ground state of initially two decoupled parts which are then joined together (local quench). Specifically we focus on the transverse-field Ising chain and compute the time dependence of the magnetization profile, $m_l(t)$, and correlation functions at the critical point, in the ferromagnetically ordered phase and in the paramagnetic phase. At the critical point we find finite-size scaling forms for the non-equilibrium magnetization and compare predictions of conformal field theory with our numerical results. In the ferromagnetic phase the magnetization profiles are well matched by predictions from a quasi-classical calculation that we describe.

Contents

1. Introduction

Non-equilibrium quantum relaxation, the dynamical evolution of a quantum mechanical system initialized in a non-eigenstate of its Hamiltonian, is a topic that has gained a lot of interest recently. Experimentally one can prepare a quantum system in such an initial state by instantaneously changing an external parameter like a field or interaction strength contained in its Hamiltonian, realizable for instance with ultracold gases (see [1]) for a review). This procedure, denoted as a quantum quench or simply quench, can be performed either globally, for instance by changing an external field or potential acting homogeneously on the whole system, or locally, for instance by changing a single interaction strength or altering a single degree of freedom. The latter are, for instance, experimentally realizable by x-ray absorption in metals [2], where the creation of a hole plays the role of a local defect, and when a conduction electron fills the hole this potential is suddenly switched off.

Global quenches have gained the most theoretical interest up to now. The first theoretical studies were performed for integrable models like quantum XY and quantum Ising spin chains [3]–[5]; later other systems were also considered: 1D Bose systems [6]–[10] and 2D superfluids [11], antiferromagnetic Heisenberg spin chains [12], 1D fermions [13, 14], the quantum sine–Gordon model [15] and Luttinger liquids [16], to name but a few. In particular for the transverse-field Ising chain, which we will consider in this paper, a pretty thorough understanding of the issue of thermalization (or absence thereof) [17]–[19] and a semi-classical quasi-particle picture (valid away from the critical point) [20] has been obtained recently. Besides studies on specific models there were also

field-theoretical investigations, in which relation with boundary critical phenomena and conformal field theory are utilized [21]–[23].

Local quenches are most straightforwardly realized by a sudden change of the interaction strength between two neighboring degrees of freedom. They became soon a tool to study the evolution of quantum entanglement between two initially independent subsystems [24]–[30]. Also work done on the transverse-field Ising system at criticality after a local quench has been analyzed [31]. Much less is known about the dynamical evolution of order parameter profiles and correlation functions in extended quantum systems after a local quench. For these one expects regions in a distance r from the defect affected by the local quench only after a time defined by the maximum group velocity for wavepackets emitted at the location of the defect, which should be reflected in the spacetime dependence of order parameter profiles. In general multi-point correlation functions are expected to display sudden changes whenever a spacetime point at which the correlation function is considered enters the light cone defined by the aforementioned maximum group velocity.

In [25] the asymptotic functional form of two-point correlation functions was computed within a conformal field theory (CFT) framework, relevant for, for example, the infinite transverse-field Ising chain at the critical point (and only there). They obey characteristic power laws in time and distance from the local quench, reminiscent of surface critical phenomena, with exponents which were predicted in [25]. What happens in finite systems (where signals can be reflected at the boundaries) with regards to spin correlations and order parameter profiles at and away from the critical point is, so far, not known. This is the question that we will try to answer in this paper.

As a model we use the transverse-field (or quantum) Ising spin chain, which is a prototypical quantum system having ordered and disordered phases as well as a quantum critical point [32]. Using free-fermionic techniques [33, 3, 32] we analyze numerically the non-equilibrium relaxation for the magnetization, the autocorrelation and the equal-time correlation function in large finite systems after a local quench. At the critical point the finite-size scaling forms for order parameter profiles will be extracted and the predictions of CFT [25] for the spatial correlation function will be checked. In the ferromagnetic phase we propose a quantitative quasi-particle concept which has been successfully applied to global quenches [20].

The structure of the paper is the following. The model and the numerical method of the calculation is introduced in section 2. Results of the calculations at the critical point, in the ferromagnetic and in the paramagnetic phases are presented in sections 3, 4 and 5, respectively. Our conclusions are summarized in section 6.

2. Model

The system we consider in this paper is the transverse-field Ising chain of finite length L with open boundaries defined by the Hamiltonian:

$$\mathcal{H} = -\tfrac{1}{2} \left[\sum_{l=1}^{L-1} J_l \sigma_l^x \sigma_{l+1}^x + \sum_{l=1}^{L} h_l \sigma_l^z \right], \tag{1}$$

in terms of the Pauli matrices $\sigma_l^{x,z}$ at site l and bond strengths J_l, which are all equal $J_l = 1$ except the central bond $J_{L/2}$, which is $J_{L/2} = 0$ for time $t \leq 0$. Similarly, the transverse

fields are homogeneous, $h_l = h$, except at the central sites, which are $h_{L/2} = h_{L/2+1} = 0$ for time $t \leq 0$ for fixed-spin boundary conditions. (For free-spin boundary conditions these are $h_{L/2} = h_{L/2+1} = h$ for time $t \leq 0$, too.) Generally we measure distances from the defect and use the variable

$$r = l - \frac{L}{2}. \tag{2}$$

The state of the system after the local quench—in the Schrödinger picture—is time-dependent:

$$|\Psi(t)\rangle = \exp(-\mathrm{i}t\mathcal{H})|\Psi_0\rangle, \tag{3}$$

and so is with an operator, say $\mathcal{O}$, which is expressed at time $t > 0$ in the Heisenberg picture as

$$\mathcal{O}(t) = \exp(-\mathrm{i}t\mathcal{H})\mathcal{O}\exp(\mathrm{i}t\mathcal{H}). \tag{4}$$

Generally one is interested in the relaxation of the local order parameter:

$$m_r(t) = \langle\Psi_0|\mathcal{O}_r(t)|\Psi_0\rangle, \tag{5}$$

at site, r or the time dependence of the autocorrelation function:

$$G_r(t, t') = \langle\Psi_0|\mathcal{O}_r(t)\mathcal{O}_r(t')|\Psi_0\rangle. \tag{6}$$

After long times, $t \gg 1$, the system is expected to relax to a stationary state, in which one measures the correlation function:

$$C_t(r_1, r_2) = \langle\Psi_0|\mathcal{O}_{r_1}(t)\mathcal{O}_{r_2}(t)|\Psi_0\rangle. \tag{7}$$

The order parameter operator of the transverse-field Ising chain in (1) is σ_l^x, which should be inserted in the formulae of the autocorrelation and the correlation functions equations (6) and (7), respectively. The local magnetization in equation (5) is given by $m_r(t) = \lim_{b\to 0_+}\ {}_b\langle\Psi_0|\sigma_r^x(t)|\Psi_0\rangle_b$, where $|\Psi_0\rangle_b$ is the ground state of the initial Hamiltonian (1) in the presence of an external longitudinal field b. According to [34] this can be written as the off-diagonal matrix element of the Hamiltonian (1):

$$m_r(t) = \langle\Psi_0|\sigma_r^x(t)|\Psi_1\rangle, \tag{8}$$

where $|\Psi_1\rangle$ is the first excited state of the initial Hamiltonian ($t < 0$). For fixed-spin boundary condition the ground state is exactly degenerate with $|\Psi_1\rangle$. In the initial state and in the thermodynamic limit, $L \to \infty$, there is spontaneous ferromagnetic order in the system, $m_r(0) > 0$, for $h < h_c = 1$. In contrast, for stronger transverse fields, $h > h_c$, the magnetization is vanishing. At the quantum critical point the magnetization vanishes as a power law: $m_r(0) \sim L^{-x_m}$, for bulk spins: $r = O(1)$, and $m_{\pm L/2}(0) \sim L^{-x_s}$, for surface spins. Here the magnetization exponent x_m and the surface magnetization exponent x_s are known exactly: $x_m = 1/8$ and $x_s = 1/2$.

The Hamiltonian in equation (1) can be expressed in terms of free fermions [33, 3, 32], which has been used in previous studies of its non-equilibrium properties [4, 17, 18]. The magnetization profile, as well as the (auto)correlation functions, can be expressed in terms of Pfaffians, which are then evaluated as the square root of an antisymmetric matrix, which has a rank $O(L)$. In the following sections we use these techniques to calculate different non-equilibrium quantities.

3. Local quenches at the critical point

At the critical point $h = J = 1$ of the Hamiltonian (1) various non-equilibrium observables are expected to display power law decay and scaling behavior. Several conjectures for local quenches in infinite systems at criticality were formulated on the basis of CFT [25], which we recapitulate for completeness in the appendix. Below we present our numerical results for the one-point (magnetization) and two-point (correlation, autocorrelation) functions, and where it is applicable we compare them with the conformal and scaling results. Additionally, in finite systems these power laws enter finite-size scaling forms which we predict on the basis of our numerical data.

One peculiarity of the finite-size dynamics after critical local quenches is the periodicity in time, as first observed for the dynamical evolution of the entanglement entropy [27, 30]. This periodicity can be understood qualitatively in terms of signals or quasi-particles emitted from the central site pair in the moment of the quench, which travel with the speed $c = 1$, constituting the light cone $x = t$, and are reflected at the boundaries of the system or wrap around the system in the case of periodic boundary conditions. The quasi-particle concept can even be made quantitative away from the critical point (in particular deep in the FM phase, $h \ll J$) as described in [18, 20] for global quenches, and in section 4 below for local quenches. But it fails to be quantitative at the critical point $h = J$, where the correlation length is infinite and hence a semi-classical theory based on individual, well-localized non-interacting excitations is inappropriate. Here scaling theory and CFT are the appropriate tools to describe the dynamics.
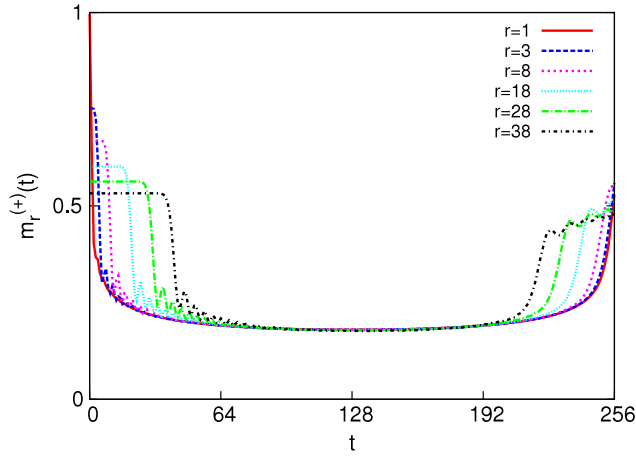
3.1. Magnetization

The relaxation of the magnetization is calculated with two different types of initial state. First, we consider an initial state with fixed spins at the defect (but the other ends of the chains are free). In this case the initial defect magnetization stays finite and one can make a direct comparison with the conjectures of conformal invariance valid for $L \to \infty$. In the second calculation in the initial state there are free boundaries, also at the defect. In this case we calculate the time dependence of the off-diagonal order parameter in equation (8), which has a vanishing initial value at the defect in the thermodynamic limit. In this setting no conformal results are available.

3.1.1. Fixed-spin boundary condition. In this section in the initial state, $t < 0$, the two half-chains are prepared with fixed spins at the boundaries: $\langle \sigma^x_{L/2} \rangle = \langle \sigma^x_{L/2+1} \rangle = 1$, which is obtained by fixing $h_{L/2} = h_{L/2+1} = 0$ in the Hamiltonian in equation (1). We use the superscript, $^{(+)}$, to refer to the fixed-spin boundary condition. The magnetization profile in the initial state is known from conformal invariance [36, 37]:

$$m^{(+)}_r(t = 0, L) \sim \left| \frac{L}{2\pi} \sin \pi \frac{2r}{L} \right|^{-x_{\mathrm{m}}} \left(\cos \pi \frac{r}{L} \right)^{x_{\mathrm{s}}}, \qquad (9)$$

which behaves close to the defect: $m^{(+)}_r(t = 0) = A|r|^{-x_{\mathrm{m}}}$, $|r| \ll L/2$. This is the well-known result by Fisher and de Gennes [38], which is also given in the appendix in equation (A.3).

Figure 1. Temporal evolution of the magnetization at the critical point after a local quench having fixed spins at the defect in the initial state in a finite system of length $L = 256$.

After the local quench, for $t > 0$, we take $h_{L/2} = h_{L/2+1} = 1$ (and $J_{L/2} = 1$) and study the evolution of the magnetization. In the limit $|r| \ll L/2$ one has results from CFT, which can be obtained by evaluating equation (A.7) with the conformal transformation in equation (A.2). This calculation leads to the result [25]

$$m_r^{(+)}(t) = \begin{cases} A|r|^{-x_{\mathrm{m}}} & t < r, \\ A\left(\dfrac{\epsilon}{t^2 - r^2}\right)^{x_{\mathrm{m}}} & t > r. \end{cases} \tag{10}$$

This can be interpreted that for $t < r$ the magnetization keeps its initial value until the quasi-particles from the defect arrive at $t = r$ and afterwards for $r \ll t \ll L/2$ the decay is given by $m_r^{(+)}(t) \sim t^{-2x_{\mathrm{m}}}$. This decay involves twice the magnetization exponent and this behavior is similar to that of the equilibrium autocorrelation function at the critical point.

In order to check the conformal result in equation (10) we have calculated the time dependence of the magnetization in finite chains of length up to $L = 256$. For the largest chain and for different values of r the relaxation of the magnetization is shown in figure 1. In agreement with the quasi-particle picture and with the results of conformal invariance the local magnetization stays unchanged until $t < r$, which is followed by a fast decrease. Due to the finite size of the system the magnetization has a finite, L-dependent limiting value and for $t > L/2$ the magnetization starts to increase.

We have studied in more detail the behavior of the magnetization at the defect: $l = L/2$, i.e. for $r = 1$. For short times, $1 \ll t \ll L/2$, the decay is compatible with the conformal prediction: $m_1^{(+)}(t) \sim t^{-1/4}$ is seen in the inset of figure 2 in which the magnetization is shown as a function of time in a log–log plot. For longer time the boundaries of the chain start to influence the relaxation and the critical defect magnetization is expected to satisfy the scaling behavior: $m_1^{(+)}(t, L) = b^{-2x_{\mathrm{m}}} m_1^{(+)}(t/b^z, L/b)$, when lengths are rescaled by a factor $b > 1$. In this relation the
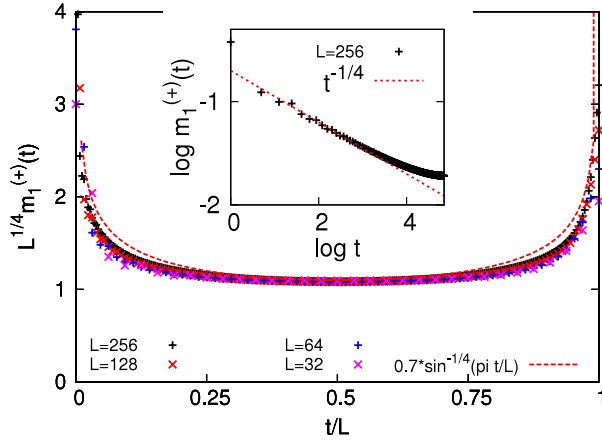
Figure 2. Temporal evolution of the magnetization at the defect after a local quench from a fixed spin at the critical point. In the main panel the scaled profiles are shown for different values of L, where the curve with the dashed line is given in equation (11). In the inset the log–log plot of $m_1^{(+)}(t, L)$ is shown for $L = 256$, where the conformal prediction for $L \to \infty$ is given by the dashed straight line.

dynamical exponent is $z = 1$ and by taking the scaling factor as $b = t$ in the limit $L \gg t$ we recover the conformal result: $m_1^{(+)}(t) \sim t^{-2x_{\mathrm{m}}}$. It is more interesting to take $b = L$, when one obtains $m_1^{(+)}(t, L) = L^{-2x_{\mathrm{m}}} \mu_1^{(+)}(t/L)$. Here the scaling function $\mu_1^{(+)}(\zeta)$ for small $\zeta = t/L$ behaves as $\mu_0^{(+)}(\zeta) \sim \zeta^{-2x_{\mathrm{m}}}$. Numerical results for the scaling function for different values of L are shown in the main panel of figure 2, which is found to be well approximated by the function $B[\sin(\pi\zeta)]^{-2x_{\mathrm{m}}}$. Thus we have the conjecture for large t and L:

$$m_1^{(+)}(t, L) \propto L^{-2x_{\mathrm{m}}} \left[\sin\left(\pi \frac{t}{L} \right) \right]^{-2x_{\mathrm{m}}}. \tag{11}$$

This result probably can be derived through CFT using the conformal transformation for finite systems, as outlined at the end of the appendix.

3.1.2. Free-spin boundary condition. Here we start the relaxation from an initial state with two free half-chains. Thus in equation (1) we have $h_{L/2} = h_{L/2+1} = 1$ and $J_{L/2} = 0$. In this settings, when no conformal results are available, we calculate the profiles of the off-diagonal order parameter, $m_r(t)$, in equation (8) in finite systems. The results are shown for $L = 128$ in figure 3.

Initially (at $t = 0$) the ground state magnetization profiles are identical and independent in both disconnected parts of the system. The functional form is known from conformal invariance [39] and the complete profile has the finite-size scaling form:

$$m_r(t = 0, L) \propto L^{-x_{\mathrm{m}}} \left| \sin \frac{2\pi r}{L} \right|^{x_{\mathrm{s}} - x_{\mathrm{m}}}. \tag{12}$$

Close to the defect, i.e. for $|r| \ll L/2$ the behavior of the profile follows from the scaling relation, that $m_r(t = 0, L) = b^{-x_{\mathrm{m}}} m_{r/b}(t = 0, L/b)$, with a rescaling factor, $b > 1$. Now
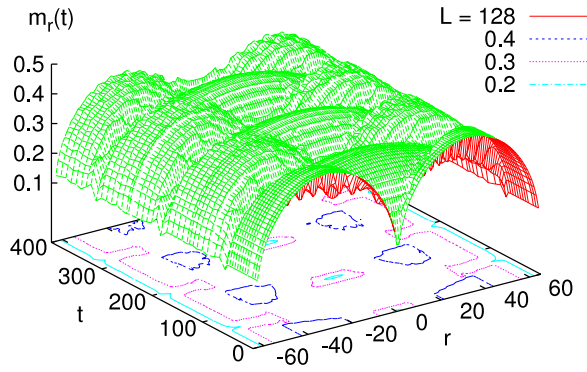
Figure 3. Temporal evolution of the local magnetization profiles at the critical point after a local quench with free boundary conditions in the initial state.
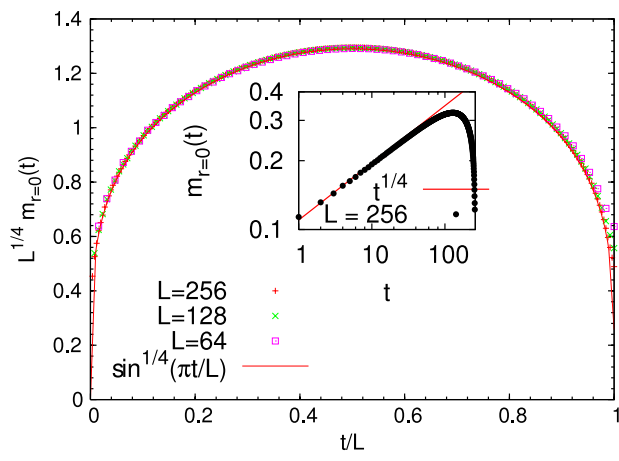
Figure 4. Scaling plot of the local magnetization at the defect, $m_0(t)$, after a local quench at criticality for different system size L. The conjectured result in equation (13) is shown by a full line. Inset: log–log plot of $m_0(t)$ versus t for $L = 256$. The straight line is proportional to $t^{1/4}$.

taking $b = L$, we arrive to the form: $m_r(t = 0, L) = L^{-x_\mathrm{m}} \tilde{m}(r/L)$, where the scaling function, $\tilde{m}(\rho)$ for small argument behaves as $\tilde{m}(\rho) \sim \rho^{x_\mathrm{s}-x_\mathrm{m}}$. This is compatible with the conformal result in equation (12), if we replace ρ by its sinusoidal extension: $\sin(2\pi\rho)$.

In figure 3 one observes a quasi-periodic time dependence of the profile with the characteristic initial double peak being exchanged against a single peak at times $T = L/2, 3L/2, \dots$ and re-occurring at times $T = L, 2L, \dots$. Let us focus first on the time dependence of the magnetization at the central site, $m_1(t, L)$, which is expected to satisfy the same type of scaling relation as $m_1^{(+)}(t, L)$, thus $m_1(t, L) = b^{-2x_\mathrm{m}} m_1(t/b, L/b)$. As before, taking $b = L$ we arrive at $m_1(t, L) = L^{-2x_\mathrm{m}} \tilde{\mu}_1(t/L)$, where the scaling function, $\tilde{\mu}_1(\zeta)$, for small argument should behave as $\tilde{\mu}_1(\zeta) \sim \zeta^{x_\mathrm{s}-2x_\mathrm{m}}$. In this way we obtain $m_1(t, L) = L^{-x_\mathrm{s}} t^{x_\mathrm{s}-2x_\mathrm{m}}$, which is in agreement with the L dependence of the magnetization at the defect at $t = 0$, see in equation (12). Furthermore we have for the relaxation for small times: $m_1(t) \sim t^{1/4}$, which agrees well with the numerical data shown in the inset of figure 4. The form of the scaling function can be conjectured using the same substitution,
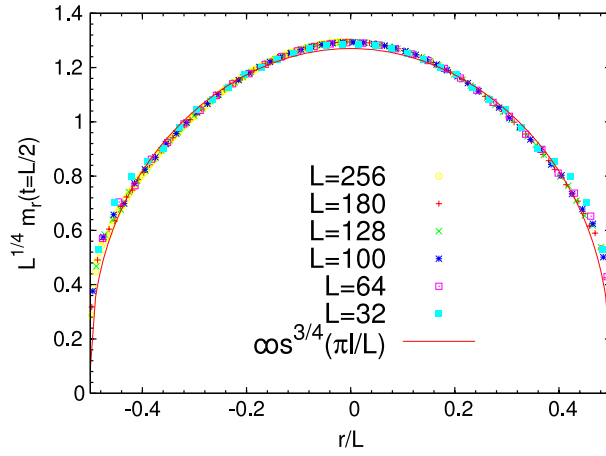
Figure 5. Scaling plot of the local magnetization $m_r(t)$ after a local quench at criticality for different system size L at time $t = L/2$, see equation (14).

$\rho \rightarrow \sin(2\pi\rho)$, as for $t = 0$. In this way we obtain

$$m_1(t, L) \propto L^{-2x_m} \left| \sin \frac{2\pi t}{L} \right|^{x_s - 2x_m}. \tag{13}$$

Figure 4 displays a corresponding finite-size scaling plot for the first period which shows a good data collapse (a corresponding scaling plot for larger values of t/L is equally good, data not shown) and thus confirms our conjecture (13), which probably can be derived rigorously from conformal invariance.

Next we consider $t = L/2$, when the profile has its maximum at $r = 0$ and it is minimal at the two ends of the chain, $r = \pm L/2$, i.e. at $l = 1$ and L. Let us consider the profile for small l and use the scaling transformation: $m_l(t/L = 1/2, L) = b^{-2x_m} m_{l/b}(t/L = 1/2, L/b)$, which leads to the result: $m_l(t/L = 1/2, L) = L^{-2x_m}\mu(l/L)$, with $b = L$. The scaling function, $\mu(y)$, for small argument is expected to behave in the same way as for $t = 0$, thus $\mu(y) \sim y^{x_s - x_m}$. Furthermore having the substitution: $y \rightarrow \sin(2\pi y)$ we arrive at the conjecture:

$$m_r(t = L/2, L) \propto L^{-2x_m} \left| \cos \frac{\pi r}{L} \right|^{x_s - x_m}, \tag{14}$$

where we use the variable r. Figure 5 displays a corresponding finite-size scaling plot which shows a good data collapse and thus supports our conjecture (14).

Finally we note that combining the scaling forms (13) and (14) the ratio $R = m_{l=L/2}^{(L)}(t = \zeta)/m_{l=\zeta}^{(L)}(t = L/2)$ is given by

$$R = \left(\sin \pi \frac{\zeta}{L} \right)^{-x_m}. \tag{15}$$

3.2. Spatial correlations

The spatial correlation function, $C_t(r_1, r_2)$ in equation (7), can be studied by CFT. For this one should evaluate the expression in equation (A.8) with the conformal mapping
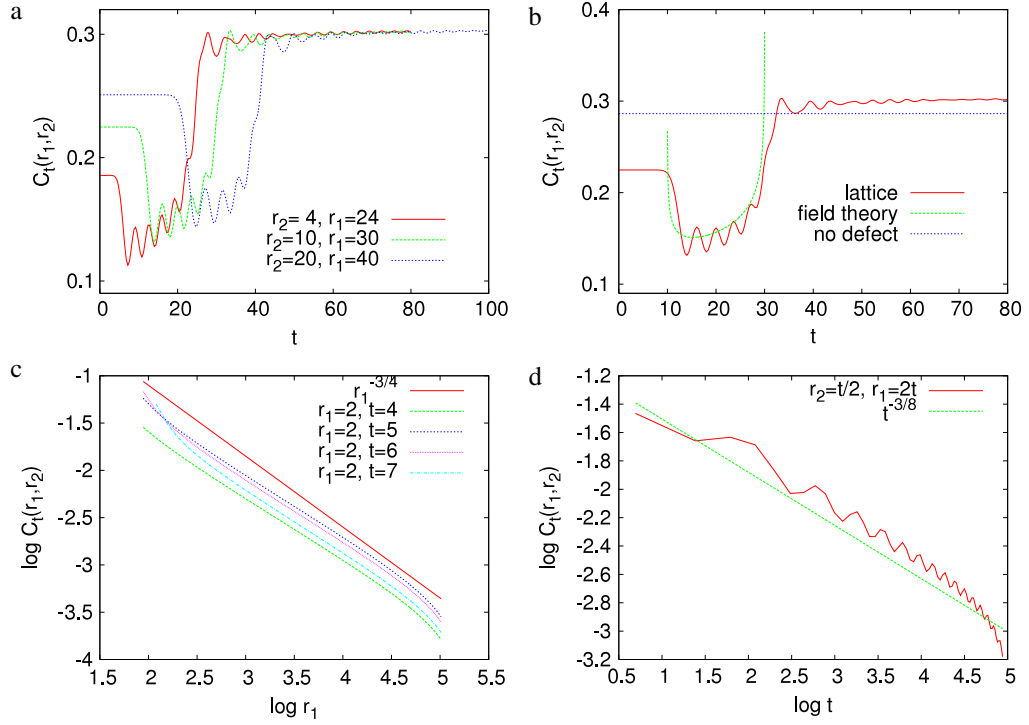
Figure 6. (a) Spatial correlation function $C_t(r_1, r_2)$ as a function of time t for both sites of reference being at the same side of the defect (i.e. $r_1 \geq r_2 > 0$). The system size is $L = 256$, as in the other panels, and in order to avoid finite-size effects, including the periodicity in time, we restrict our calculations to $r_1, r_2, t \ll L$. (b) Comparison of the data of (a) for $r_2 = 10$, $r_1 = 30$ with the CFT result (16). (c) $C_t(r_1, r_2)$ in the intermediate-time regime ($r_2 < t < r_1$) for small r_2 and t as a function of r_1. In the limit $r_1 \to \infty$ this should approach $r_1^{-3/4}$ according to the CFT result (17). (d) $C(r_1, r_2; t)$ in the intermediate-time regime for $r_2 = t/2$ and $r_1 = 2t$ as a function of t that should decay as $t^{-3/8}$ according to the CFT result (18).

in equation (A.2). In this case various analytical predictions have been obtained for an infinite system in the continuum limit [25]. In this section we will compare our results for finite lattice systems with free boundaries with these predictions. We note that before the quench the two halves of the system are disconnected and free, i.e. $h_{L/2} = h_{L/2+1} = 1$ and $J_{L/2} = 0$. Without the restriction of generality we take $r_1 > |r_2| > 0$ and consider two cases: (1) both sites of the reference are at the same side of the defect ($r_2 > 0$), and (2) the two sites are at different sides of the defect ($r_2 < 0$).

Case 1: $r_2 > 0$. For short times, $t < r_2$ ($<r_1$), the behavior of the correlation function can be obtained in the quasi-particle picture. In this case the quasi-particles (which can be called signals) starting at the defect and propagating with a speed $v = 1$ do not reach any point of reference. Thus the correlations keep their initial value: $C_t(r_1, r_2) = C_0(r_1, r_2) \propto |r_1 - r_2|^{-2x_m}$. This result also follows from CFT and is consistent with our numerical data depicted in figures 6(a) and (b).

For intermediate times, $r_2 < t < r_1$, the signals reach the closest site at r_2 but not yet the remote site at r_1, see figures 6(a) and (b). The prediction from CFT [25] is

$$C_t(r_1, r_2) = \left\{ \frac{(r_1 + r_2)(r_2 + t)\epsilon}{(r_1 - r_2)(r_1 - t)4r_1(t^2 - r_2^2)} \right\}^{x_{\mathrm{m}}} F\left(\frac{2r_1(r_2 + t)}{(r_1 + r_2)(r_1 + t)} \right) \quad (16)$$

with $F(\eta)$, defined in equation (A.6) for free boundary conditions, i.e. with $-$ sign, which behaves as $F(\eta) \sim \sqrt{\eta}$ for $\eta \to 0$ and ϵ is the regularization parameter in equation (A.2). In figure 6(b) a comparison with our numerical data for a specific r_1 and r_2 is shown. As expected for a lattice model our data display characteristic oscillations in the considered regime around the monotonic continuum result (16).

For a more quantitative comparison we first look at the asymptotic behavior of $C_t(r_1, r_2)$ for fixed small t and r_2. The CFT predicts according to (16) and (A.6)

$$C_t(r_1, r_2) \propto r_1^{-2x_{\mathrm{m}} - x_{\mathrm{s}}} = r_1^{-3/4} \qquad \text{for } t < r_2 \ll r_1 \quad (17)$$

which agrees well with our lattice result as shown in figure 6(c). Moreover, for fixing the ratios $\rho_2 = r_2/t < 1$ and $\rho_1 = r_1/t > 1$, (16) and (A.6) predict in the limit $t \to \infty$

$$C_t(r_1, r_2) \propto t^{-3x} = t^{-3/8} \qquad \text{for } \rho_2 < 1 \quad \rho_1 > 1 \quad t \to \infty. \quad (18)$$

This is also consistent with our finite lattice data as seen in figure 6(d) for $\rho_2 = 1/2$ and $\rho_1 = 2$.

In the long-time regime, for $t > r_1$ the signals have also reached the remote site at r_1, and both points of reference have the information on the joining of the two halves of the system. Consequently $C_t(r_1, r_2)$ approaches a time-independent value (cf figures 6(a) and (b)), given by the equilibrium bulk correlation function, which is proportional to $|r_1 - r_2|^{-2x_{\mathrm{m}}}$.

Case 2: $r_2 < 0$, i.e. the two reference sites are at different sides of the defect. Initially, at $t = 0$, the two magnetization operators are located in separate, independent subsystems. Thus their correlations should vanish. As long as after the quench no signal reaches the site at r_2 (i.e. for $t < |r_2|$) the correlation function should be expected to be zero. (Strictly speaking $C_t(r_1, r_2)$ can be exponentially small, the only contributions coming from signals propagating outside the 'light cone'.) This is clearly visible in our results shown in figure 7(a). Surprisingly this disagrees with the CFT result [25] which predicts

$$C_t(r_1, r_2) = \frac{1}{|4r_1 r_2|^{x_{\mathrm{m}}}} F\left(\frac{\epsilon^2 r_1 |r_2|}{(r_1^2 - t^2)(r_2^2 - t^2)} \right) \qquad \text{for } t < |r_2|. \quad (19)$$

This could be rectified by setting $\epsilon = 0$, but this would be at variance with the results for $r_2 > 0$, for which the regularization parameter should be non-vanishing. The problem with the conformal derivation could be related to the fact that, in the transformation, (A.2) points in the z plane with $\mathrm{Re}(z_2) = r_2 < 0$ and $|r_2| \gg \epsilon$ are transformed to $|w_2| \ll \epsilon$. However, the scaling form of the correlation function in the semi-infinite w plane is valid only in the continuum limit, i.e. for $\mathrm{Re}(w_2) \gg 1$.

After the signals reach the site at r_2, i.e. for $|r_2| < t < r_1$, the CFT prediction is [25]

$$C_t(r_1, r_2) = \left(\frac{(r_1 + r_2)(r_2 + t)\epsilon}{(r_1 - r_2)(r_1 - t)4r_1(t^2 - r_2^2)} \right)^{x_{\mathrm{m}}}$$

$$\times F\left(\frac{2r_1(r_2 + t)}{(r_1 + r_2)(r_1 + t)} \right) \qquad \text{for } |r_2| < t < r_1. \quad (20)$$
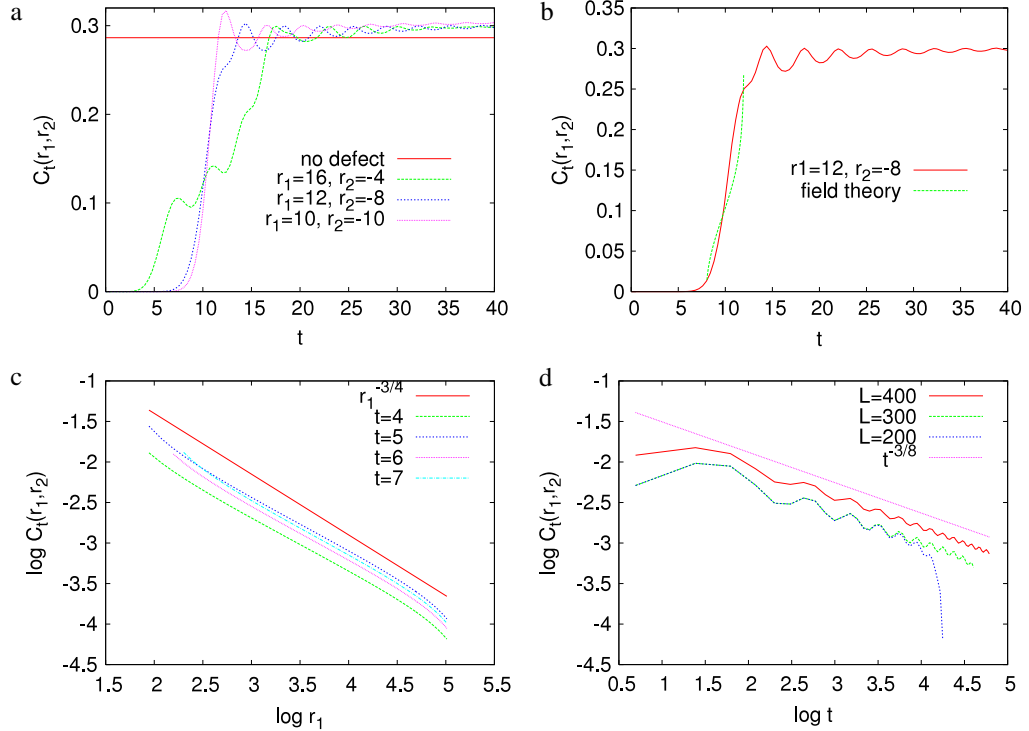
Figure 7. (a) Spatial correlation function $C_t(r_1, r_2)$ as a function of time t for the two sites of reference being at different sides of the defect: $r_1 > 0$ and $r_2 < 0$ ($r_1 \geq |r_2|$). The system size is $L = 256$, as in the other panels. (b) Comparison of $C_t(r_1, r_2)$ with the CFT result (20). (c) $C_t(r_1, r_2)$ for small $|r_2|$ and t as a function of r_1. In the limit $r_1 \rightarrow \infty$ this should approach $r_1^{-3/4}$ according to the CFT result (17). (d) $C_t(r_1, r_2)$ for $r_2 = t/2$ and $r_1 = 2t$ as a function of t that should decay as $t^{-3/8}$ according to the CFT result (18).

In figure 7(b) a comparison with our numerical data for a specific r_1 and r_2 is shown. As found also in case 1, for a lattice model our data display characteristic oscillations in the considered regime around the monotonic continuum result (20).

For fixed small t and r_2 the CFT predicts according to (20) and (A.6) again for $C_t(r_1, r_2)$ the asymptotic r_1 behavior (17) as in the case $r_2 > 0$. This agrees well with our lattice result as shown in figure 7(c). Moreover, for fixed $\rho_2 = r_2/t > -1$ and $\rho_1 = r_1/t > 1$ (20) predicts in the limit $t \rightarrow \infty$ the same asymptotic t behavior (18) as in the case $r_2 > 0$. This is also in agreement with our lattice result as shown in figure 7(d). Finally for $t > r_1$ the signal has also reached the site at r_1 and $C_t(r_1, r_2)$ approaches again the time-independent equilibrium bulk value (cf figure 7), which is proportional to $|r_1 - r_2|^{-2x_m}$.

Summarizing our results confirm the predictions of the CFT [25] for the spatial correlation after a local quench at the critical point, except for the case $r_2 < 0$, $t < |r_2|$.

3.3. Autocorrelations

We have also calculated the autocorrelation function, $G_r(t, 0)$, as defined in equation (6). In the following for simplicity we shall omit the second argument and use the notation
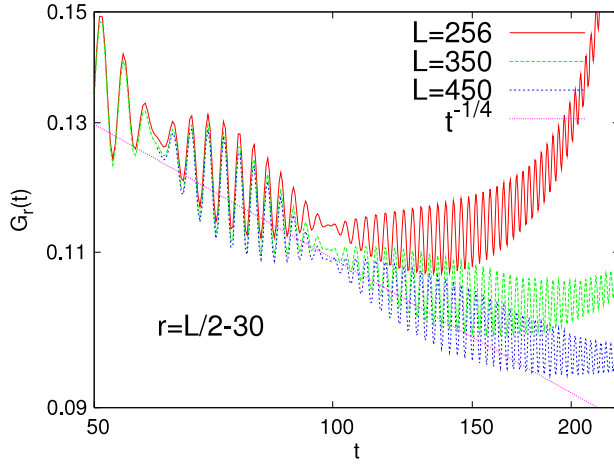
Figure 8. Autocorrelation function $G_r(t)$ after a critical quench for different system sizes. The straight line corresponds to the equilibrium power law $t^{-1/4}$.

$G_r(t)$. Using the quasi-particle picture we have the following expectations. Before the signal reaches the reference point, $t < r$, the autocorrelation function is the same as in the equilibrium bulk system, thus asymptotically $G_r(t) \propto t^{-2x_\mathrm{m}/z} = t^{-1/4}$. For $t > r$, when the signal has passed the reference point the equilibrium bulk decay of $G_r(t)$ should continue. Thus in the complete time window this behavior is observable.

Our lattice results in figure 8 are in agreement with these expectations. In a finite lattice of length L the autocorrelation function has a minimal value of $\sim L^{-1/4}$.

4. Quench in the ferromagnetic phase

In equilibrium in the ferromagnetic (FM) phase ($h < 1$) there is spontaneous order and the bulk, m_b, and the surface, m_s, magnetizations are given by

$$m_\mathrm{b} = (1 - h^2)^{x_\mathrm{m}\nu}, \qquad m_\mathrm{s} = (1 - h^2)^{x_\mathrm{s}\nu}, \tag{21}$$

respectively (the correlation length exponent is $\nu = 1$). The magnetization profile has an exponential variation in the surface region, the size of which is given by $\xi_\mathrm{s} \sim (1 - h)^{-1}$, close to the critical point. Here we follow the same protocol as in section 3.1.2: for $t < 0$ we cut the system into two halves with free boundary conditions, which are then (at $t = 0$) joined together with the coupling $J_{L/2} = J = 1$. We measure the temporal evolution of the magnetization profile, $m_r(t)$, as defined in equation (8). The finite lattice results are depicted in figure 9 for $h = 0.5$ and $L = 128$. In the initial state the magnetization profile ($m_r(t = 0)$) is essentially constant and given by m_b, except close to the boundaries and to the center. For $t > 0$ one observes again a quasi-periodic pattern and the period of time $T(h)$ is found to increase with increasing L and decreasing field h. It turns out that the spatio-temporal evolution of the profile can be understood even quantitatively within a quasi-classical picture, which we describe below.

As elaborated in [20] within the FM phase and in particular for small h the dynamics of the local order parameter and correlation functions in a system with boundaries after a global quench is very well described by a semi-classical theory based on kinks, i.e. pairs
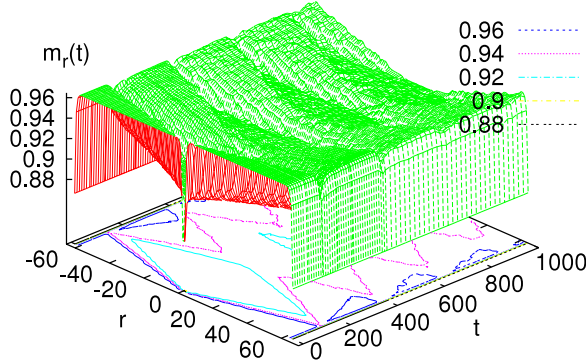
Figure 9. Temporal evolution of the local magnetization profiles after a local quench within the ordered (FM) phase, here $h = 0.5$ and $L = 128$.

of anti-parallel spin neighbors, moving with a velocity $\pm v_\mathrm{p}$ through the system. These kinks are quasi-particles (QPs) with an energy given by the dispersion relation of the Hamiltonian (1)

$$\epsilon_\mathrm{p} = \sqrt{1 + h^2 - 2h\cos(p)} \tag{22}$$

with $p = (2n - 1)\pi/2L$ $(n = 1, \ldots, L)$ and the QP velocity

$$v_\mathrm{p} = \frac{\partial \epsilon_\mathrm{p}}{\partial p} = \frac{h\sin(p)}{\epsilon_\mathrm{p}}. \tag{23}$$

The maximum velocity is given by

$$v_\mathrm{max}^2 = \left[\sqrt{(1 + h^2)^2 + 12h^2} - (1 + h^2)\right]/6, \tag{24}$$

for small h it is $v_\mathrm{max} \approx h$.

Consider now a QP, or kink, with momentum p. It moves uniformly with velocity v_p until it reaches one of the boundaries, where it is reflected and moves with velocity $-v_\mathrm{p}$ thereafter, and so forth. The trajectory of the kink is periodic in time, after a time $2T_\mathrm{p}$ with

$$T_\mathrm{p} = L/v_\mathrm{p} \tag{25}$$

(including a reflection at the right and left boundary) it returns to the starting point x_0 with the initial direction and velocity v_p. After a global quench QPs emerge pairwise at random positions x_0 with velocities $+v_\mathrm{p}$ and $-v_\mathrm{p}$ [17, 20] and therefore we assume that, after the local quench studied here, QPs emerge also pairwise, but exclusively at the central site, where the defect is located before the quench.

The time-dependent decay of the local magnetization $m_r(t)$ at a position r is then determined by the probability q with which any given kink trajectory passes until time t the site r an odd (!) number of times: each passage of one of the two trajectories flips the spin at site r and an even number of flips does not change the magnetization of site r. Once $q(t)$ is known the magnetization is given by [20]

$$m_r(t) = m_r(t = 0)\exp(-2q(t)). \tag{26}$$

The probability $q(t)$ is expressed as

$$q(t) = \frac{1}{\pi} \int_0^\pi \mathrm{d}p \, f_\mathrm{p}(h) \, q_\mathrm{p}(t) \tag{27}$$

where $q_\mathrm{p}(t)$ is the probability that any given QP trajectory passes the site r an odd number of times and $f_\mathrm{p}(h)$ is the probability with which QPs with momentum p are generated (per site), and we assume that it is identical to f_p after a global quench. This is given for small h as [20]

$$f_\mathrm{p}(h) = \tfrac{1}{4} h^2 \sin^2(p). \tag{28}$$

To calculate q_p one concentrates first on times $t < 2T_\mathrm{p}$ and on lattice site $r < 0$; the whole profile is of course symmetric with respect to a reflection at the center $m_r(t) = m_{-r}(t)$. The QPs emerging at the central site $r = 1$ and moving to the left ($v_\mathrm{p} < 0$) pass the site r two times (once before the reflection at the left boundary and once after the reflection) before they return (now with $v_\mathrm{p} > 0$) to their starting point. These two times are $t_1 = |r|/v_\mathrm{p}$ and $t_2 = T_\mathrm{p} - t_1$. Therefore the probability that this QP trajectory passes r at times $t < T_\mathrm{p}$ exactly once is

$$q_\mathrm{p}^- = \begin{cases} 0 & t < t_1 \\ 1 & t_1 < t < t_2 \\ 0 & t_2 < t < T_\mathrm{p}. \end{cases} \tag{29}$$

The associated partner (of the QP pair) that moves to the right ($v_\mathrm{p} > 0$) passes the site r only after reflection at the right boundary and returns to the starting point, at times $t_3 = T_\mathrm{p} + t_1$ and $t_4 = 2T_\mathrm{p} - t_1$. Therefore the probability that this QP trajectory passes r at times $t < 2T_\mathrm{p}$ exactly once is

$$q_\mathrm{p}^+ = \begin{cases} 0 & t < t_3 \\ 1 & t_3 < t < t_4 \\ 0 & t_4 < t < 2T_\mathrm{p}. \end{cases} \tag{30}$$

For $t > 2T_\mathrm{p}$ one makes use of the T_p-periodicity of $q_\mathrm{p}(t)$:

$$q_\mathrm{p}(t + 2nT_\mathrm{p}) = q_\mathrm{p}(t), \qquad (n = 1, 2, \ldots). \tag{31}$$

With (27)–(31) one obtains $m_l(t)$ via numerical integration (or summation over the discrete p values for a lattice of finite size L), where we take the exact profile before the quench ($m_l(t = 0)$).

In figure 10 the comparison of this QP calculation with our exact data is shown. Figure 10(a) displays the dynamical evolution of the local magnetization at $h = 0.2$ close to the defect. The system size, $L = 256$, is sufficiently large such that the boundary effects are not yet visible for the times shown and the data are representative for an infinite system. One sees that the initial magnetization drop at the defect (the defect spins are surface spins at $t = 0$) is quickly filled and the profile approaches a constant magnetization $\tilde{m}_\mathrm{b} = \lim_{L,t\to\infty} m_r(t)$. Since the probability $q_\mathrm{p}(t)$ for a QP with momentum p to pass any site in the bulk is 1 in the limit $L \to \infty$ and $t \to \infty$ the bulk magnetization is predicted by the QP picture, according to (27) and (26), to be

$$\tilde{m}_\mathrm{b} = m_\mathrm{b} \exp(-1/\xi), \tag{32}$$

15
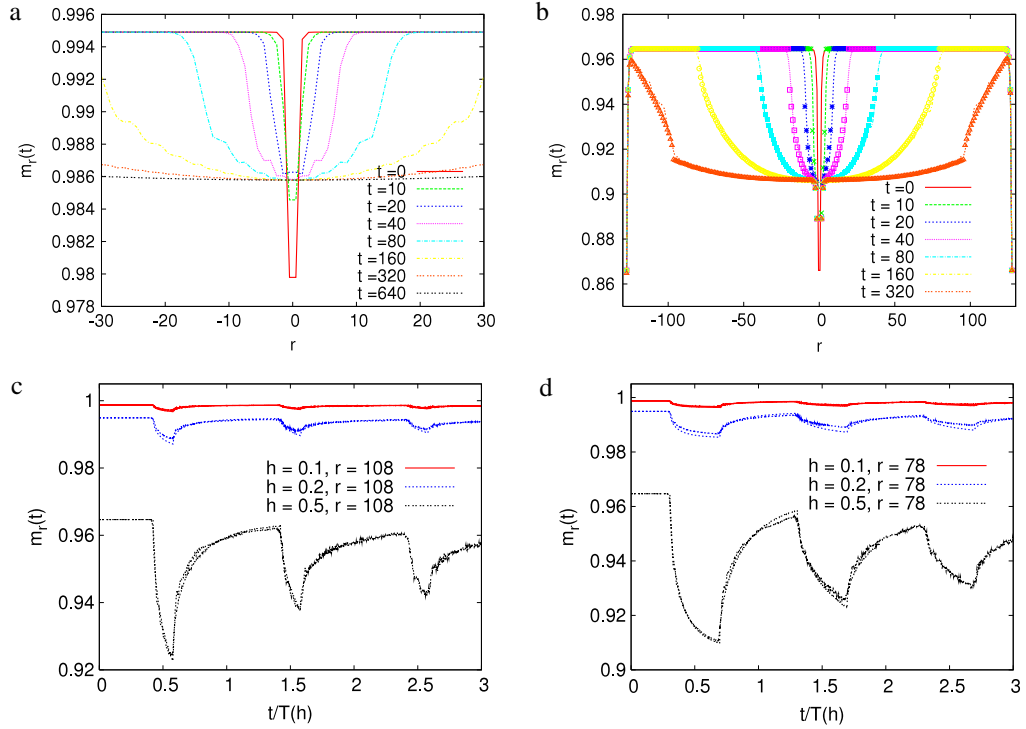
Figure 10. Local order parameter $m_l(t)$ within the FM phase ($h < 1$) and comparison with QP calculation. (a) $m_r(t)$ at $h = 0.2$ as a function of the distance r from the defect for different fixed times t. (b) $m_l(t)$ at $h = 0.5$ as a function of l for different fixed times ($L = 256$, the defect is at $l = 128$). The full lines are the exact data and the points are the predictions of the QP calculation. (c) and (d) $m_l(t)$ for different fields $h < 1$ as a function of the rescaled time $t/T(h)$, where $T(h) = L/v_{\max}(h) = L/h$, i.e. $T(h = 0.5) = 512$, $T(h = 0.2) = 2560$ and $T(h = 0.1) = 5120$. The exact data and the QP prediction can be discriminated by the smoother behavior of the latter.

with

$$\frac{1}{\xi} = \frac{1}{\pi} \int_0^\pi \mathrm{d}p \, f_\mathrm{p}(h). \tag{33}$$

ξ is identical to the non-equilibrium correlation length measured during global quench [17]–[20]. For $f_\mathrm{p}(h)$ as in equation (28), which is exact for small h it is given by $1/\xi = h^2/4$. For larger values of h corrections to the kink-like excitations should by summed, which leads to the value [5, 19] $1/\xi = -\ln[(1 + \sqrt{1 - h^2})/2]$. For $h = 0.2$ one gets $\tilde{m}_\mathrm{b} = 0.985$ which agrees well with the approximately constant magnetization at $t = 640$ in figure 10(a). We checked that also for larger values of h the QP prediction for the asymptotic bulk magnetization $\tilde{m}_\mathrm{b}$ in equation (32) is good.

Figure 10(b) compares the exact data for the local magnetization profile of a finite system for different times after the quench with those of the QP prediction at $h = 0.5$. The agreement is very good for the times shown and a few sites away from the defect ($r = |L/2 - l| > 5$). The rapid filling of the initial sharp dip of the profile at the center (see figure 10(a)) is not correctly captured by the present QP picture. To understand
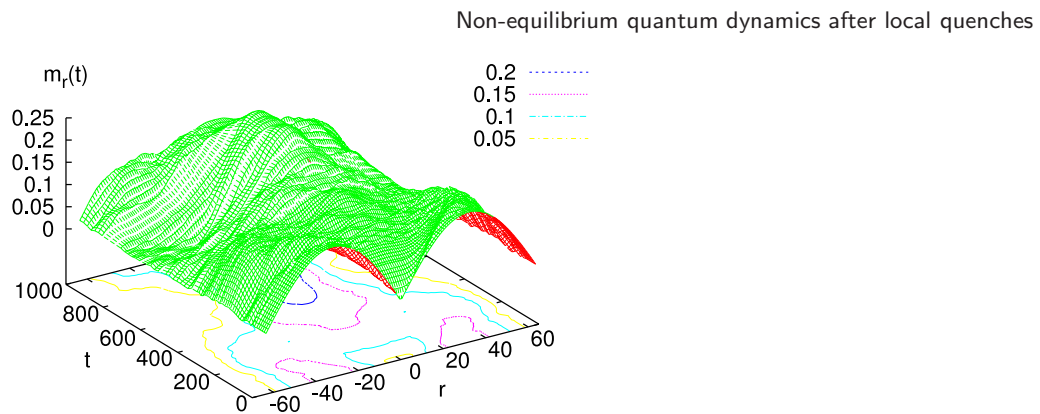
Figure 11. Temporal evolution of the local magnetization profiles after a local quench within the disordered (PM) phase, here $h = 2$, $L = 128$.

this process one should assume that the QPs are emitted in a region of size ξ_s around the defect and these QPs are quantum entangled and these correlated particles are responsible for the rapid increase of the magnetization at the defect.

The predicted (quasi)-period is governed by the maximum QP velocity and given by

$$T(h) = L/v_{\max} \approx L/h. \tag{34}$$

This agrees well with the dynamical behavior of $m_l(t)$ shown in figures 10(c) and (d) displaying the exact data and the QP prediction for $m_l(t)$ at fixed sites l for different fields $h < 1$ as a function of the rescaled time $t/T(h)$. The agreement for the sites shown is good; at longer times close to the defect ($l \approx L$) deviations occur (see figure 10(d)) due to the mechanism described above.

5. Quench in the paramagnetic phase

In the paramagnetic phase ($h > 1$) the magnetization vanishes in the infinite system, but in a finite system there is a finite, L-dependent magnetization. Its temporal evolution for $h = 2$ is depicted in figure 11 for $L = 128$. In contrast to the dynamics at the critical point (cf figure 3) the evolution of $m_l(t)$ is not periodic in the paramagnetic phase and approaches a stationary profile characteristic for the system without defect.
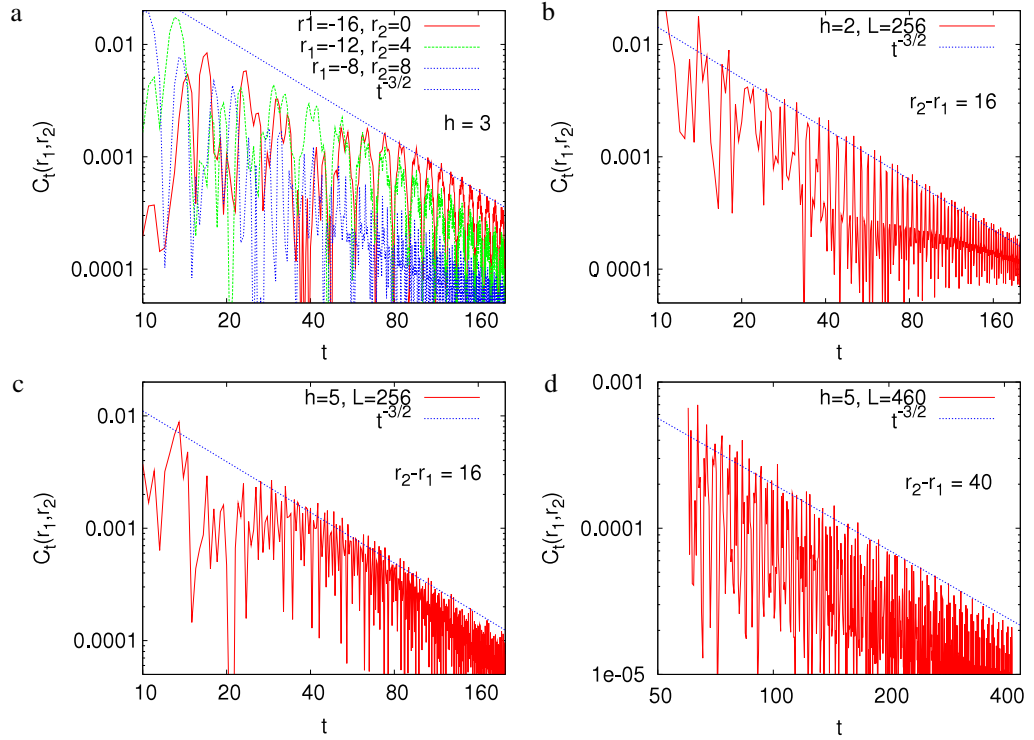
Our results for the spatial correlation function $C_t(r_1, r_2)$ within the paramagnetic phase are depicted in figure 12. We find that for fixed r_1 and r_2 an asymptotic power law in t with an exponent close to $3/2$:

$$C_t(r_1, r_2) \propto t^{-3/2} \qquad \text{for } t \gg r_1, |r_2|, \tag{35}$$

independent of r_1 and r_2. This is remarkable, in so far that it displays an algebraic time dependence away from the critical point, exclusively generated by the local quench. Note that without the quench $C_t(r_1, r_2)$ is time-independent and decays exponentially with $|r_1 - r_2|$: $C_t(r_1, r_2) \propto \exp(-|r_1 - r_2|/\xi)$.

In contrast to the spatial correlation function the autocorrelation function $G_t(r)$ is less influenced by the local quench: we find that for a local quench within the paramagnetic phase it follows a power law as in the ground state without a defect, i.e.

$$G_t(r) \propto t^{-1/2}. \tag{36}$$

17

Figure 12. Spatial correlation function $C_t(r_1, r_2)$ as a function of t for local quenches in the paramagnetic phase ($h > 1$) in a log–log plot. The straight lines correspond to the power law $t^{-3/2}$. (a) Different pairs of (r_1, r_2) with the same spatial difference at $h = 3$ (L is 256). (b) $h = 2$, $L = 256$. (c) $h = 5$, $L = 256$ and (d) $h = 5$, $L = 460$.

6. Conclusions

We have studied the temporal evolution of different observables in the transverse-field Ising chain following a local quench: for $t < 0$ the system consisted of two disconnected halves which are joined together for $t > 0$ with the uniform bulk coupling, $J_{L/2} = 1$. We have measured the magnetization profile, $m_r(t)$, as well as the correlation, $C_t(r_1, r_2)$, and the autocorrelation function, $G_r(t_1, t_2)$. We have concentrated on the properties of local quench in the critical state, but some calculations are also performed in the ferromagnetic and in the paramagnetic phases, too.

For critical local quench several conjectures for $m_r(t)$ and $C_t(r_1, r_2)$ have been obtained using CFT, which are valid in the thermodynamic limit and in the continuum approximation. Our exact finite lattice results have confirmed the conformal conjectures, except for the early time behavior of the correlation function in which the two reference points are at different sides of the defect. We have also studied systematically the finite-size effects, in particular we predicted the form of the magnetization profiles, both in space equation (14) and time equation (13), which probably can be derived within CFT, too.

The dynamics of the order parameter profile as well as correlation functions after local quenches within the ordered (ferromagnetic) phase can be quantitatively described with a semi-classical theory based on quasi-particles, which are kink-like excitations created in

the moment of the quench at the defect. They move ballistically with an energy-dependent velocity and cause the dynamic reduction of the order parameter in the system. In the ferromagnetic phase this type of semi-classical calculation has led to exact results, at least for small transverse fields, $h \ll 1$. We expect, however, that following the same method as for global quenches [20], one can sum the higher-order contributions and obtain exact results for the stationary value of the magnetization profile for a general value of $h < 1$. This involves the non-equilibrium correlation length, ξ as defined after global quenches, see equation (32).

Whereas local quenches in the ferromagnetic phase lead to quasi-periodic time dependence of the order parameter profiles due to non-interacting quasi-particles being reflected at the boundaries local quenches within the paramagnetic phase cause a quite different dynamics: the local order parameter approaches rather quickly a stationary profile characteristic for the ground state of the final Hamiltonian after the quench. Probably it is possible to formulate a quantitative quasi-particle theory for local quenches in the paramagnetic phase along the lines of [40], too, which remains as an interesting perspective for future work.

Our investigations can be extended and generalized in different directions. First, one could consider other quantum spin chains, for which similar conformal conjectures at the critical point are expected to hold as for the transverse-field Ising chain. Next, it would be interesting to study local quenches in non-integrable models, too. Away from the critical point in the ferromagnetic phase the relation in equation (32) is expected to be valid and in this way one can measure the non-equilibrium correlation length in an independent procedure. A second way to generalize our results is to use different forms of the local quench. One possibility is to use a non-zero defect coupling between the two subsystems in the initial state and/or to have a non-uniform defect coupling, $J_{L/2} \neq J = 1$, in the final state. In the transverse-field Ising chain the local critical exponents are a continuous function of the strength of the defect [41]–[43], so that x_s for a decoupled system should be replaced by a defect exponent, x_d. Finally, we can also study local defects with a more complicated structure, which involves several lattice sites.

Acknowledgments

Appendix: Conformal field theory for local quenches at the critical point

Here we recapitulate the basic results by Calabrese and Cardy [25] about the use of CFT for local quenches at the critical point. The system is represented in a spacetime region with coordinates (r, t) and the two parts of the chain are decoupled for $t < 0$ and these are joined at $t = 0$ and we measure the properties of the system at $t > 0$. The expectational value of the local magnetization operator in equation (5) can be written in
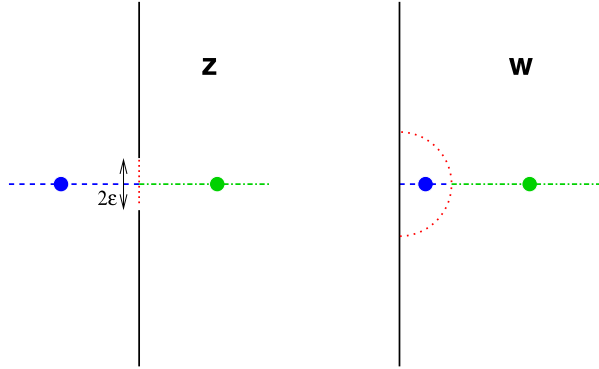
Figure A.1. Spacetime region $z = r + \mathrm{i}\tau$ with two cuts starting at $\pm\mathrm{i}\epsilon$ (left) which is mapped to the half-plane w through the conformal transformation in equation (A.2). At the end of the calculation one should take $\tau \to \mathrm{i}t$.

the path-integral formalism as

$$m_r(t) = Z^{-1} \langle \Psi_0 | \exp(-\mathrm{i}t\mathcal{H} - \epsilon\mathcal{H}) \mathcal{O}_r \exp(\mathrm{i}t\mathcal{H} - \epsilon\mathcal{H}) | \Psi_0 \rangle \qquad (A.1)$$

with the normalization: $Z = \langle \Psi_0 | \exp(-2\epsilon\mathcal{H}) | \Psi_0 \rangle$ and the damping factors, $\exp(-\epsilon\mathcal{H})$, are introduced to have the path integral absolutely convergent. A similar path integral is used to evaluate the correlation function in equation (7). For global quenches the path integral in equation (A.1) is evaluated in imaginary time, τ, in which the field, Ψ, takes the boundary value Ψ_0 at $\tau_1 = -\epsilon$ and $\tau_2 = \epsilon$. For local quench the path integral is evaluated in a spacetime region in which the physical separation of the two subsystems corresponds to two cuts on the imaginary time axis, starting at $\pm\mathrm{i}\epsilon$, see the left panel of figure A.1. Here the operator is inserted at imaginary time, τ. During the course of the calculation we consider τ as a real variable and only at the very end we continue it to its actual complex value. In this way the quantum quench dynamics of a chain is calculated with the methods of equilibrium statistical physics of two-dimensional classical systems in the spatial geometry shown in the left panel of figure A.1. At the critical point the two-dimensional classical system is expected to be conformally invariant, which can be used to simplify largely the calculation. For this we use the Joukowsky transformation:

$$w = \frac{z}{\epsilon} + \sqrt{\left(\frac{z}{\epsilon}\right)^2 + 1}, \qquad z = \epsilon\frac{w^2 - 1}{2w}, \qquad (A.2)$$

and map the $z = r + \mathrm{i}\tau$ plane into the half-plane, $\mathrm{Re}\, w > 0$. This is illustrated in figure A.1. At the boundaries of the slits in the z plane as well as at the surface of the w plane one should impose boundary conditions, which can be either free or fixed-spin boundary conditions. In the w plane the asymptotic form of the one- and two-point functions are generally known due to conformal invariance [35]–[37], [39]. For example the local magnetization for the fixed-spin boundary condition is given by

$$m^{(+)}(w) = A\,[\mathrm{Re}\, w]^{-x_{\mathrm{m}}} \qquad (A.3)$$

with a normalization constant, A. On the other hand, the two-point function in the

half-plane is known to be written in the form

$$G(w_1, w_2) = \left(\frac{|w_1 + \bar{w}_2||w_2 + \bar{w}_1|}{|w_1 - w_2||\bar{w}_2 - \bar{w}_1||w_1 + \bar{w}_1||w_2 + \bar{w}_2|} \right)^{x_{\mathrm{m}}} F(\eta) \qquad (A.4)$$

with

$$\eta = \frac{|w_1 + \bar{w}_1||w_2 + \bar{w}_2|}{|w_1 + \bar{w}_2||w_2 + \bar{w}_1|}. \qquad (A.5)$$

Here $F(\eta)$ is known for the Ising universality class being

$$F(\eta) = (\sqrt{1 + \sqrt{\eta}} \pm \sqrt{1 - \sqrt{\eta}})/\sqrt{2} \qquad (A.6)$$

and the sign $\pm$ is $+$ for fixed boundary conditions and $-$ for free ones. These results are then transformed back to the z plane using the conformal mapping in equation (A.2). Under a general conformal transformation, $w \to w(z)$, the local magnetization is transformed as

$$m^{(+)}(z_1) = \left[\left| \frac{\mathrm{d}w}{\mathrm{d}z} \right|_{z_1} \right]^{x_{\mathrm{m}}} m^{(+)}(w_1) \qquad (A.7)$$

whereas the two-point function follows the relation

$$G(z_1, z_2) = \left[\left| \frac{\mathrm{d}w}{\mathrm{d}z} \right|_{z_1} \left| \frac{\mathrm{d}w}{\mathrm{d}z} \right|_{z_2} \right]^{x_{\mathrm{m}}} G(w_1, w_2). \qquad (A.8)$$

The results obtained in equations (A.7) and (A.8) are then analytically continued as $\tau \to \mathrm{i}t$.

We note that the results obtained through the mapping in equation (A.2) are valid for infinitely long chains, i.e. for $L \to \infty$. For a large, but finite, chain the spacetime geometry, as illustrated in the left panel of figure A.1 is modified to a vertical strip of width L having the slits at the center. This type of geometry is mapped into the half-plane, $\mathrm{Re}\, w > 0$, through a Schwarz–Christoffel transformation. In this case the calculations can be most easily performed if at all boundaries we have the same type of boundary conditions [30]. Having different boundary conditions, such as for the magnetization with fixed-free boundary conditions in section 3.1.1, one should also consider boundary condition changing operators, which will generally complicate the calculation a lot.

References

[1] Bloch I, Dalibard J and Zwerger W, 2008 *Rev. Mod. Phys.* **80** 885
[2] Mahan G D, 1990 *Many-Particle Physics* (New York: Plenum)
[3] Barouch E and McCoy B, 1970 *Phys. Rev.* A **2** 1075
    Barouch E and McCoy B, 1971 *Phys. Rev.* A **3** 786
    Barouch E and McCoy B, 1971 *Phys. Rev.* A **3** 2137
[4] Iglói F and Rieger H, 2000 *Phys. Rev. Lett.* **85** 3233
[5] Sengupta K, Powell S and Sachdev S, 2004 *Phys. Rev.* A **69** 053616
[6] Rigol M, Muramatsu A and Olshanii M, 2006 *Phys. Rev.* A **74** 053616
[7] Rigol M, Dunjko V, Yurovsky V and Olshanii M, 2007 *Phys. Rev. Lett.* **98** 50405
[8] Kollath C, Läuchli A and Altman E, 2007 *Phys. Rev. Lett.* **98** 180601
    Läuchli A M and Kollath C, 2008 *J. Stat. Mech.* P05018
[9] Cramer M, Dawson C M, Eisert J and Osborne T J, 2008 *Phys. Rev. Lett.* **100** 030602

[10] Roux G, 2009 *Phys. Rev.* A **79** 021608
[11] Mathey L and Polkovnikov A, 2010 *Phys. Rev.* A **81** 033605
[12] Barmettler P, Punk M, Gritsev V, Demler E and Altman E, 2009 *Phys. Rev. Lett.* **102** 130603
Barmettler P, Punk M, Gritsev V, Demler E and Altman E, 2010 *New J. Phys.* **12** 055017
[13] Manmana S R, Wessel S, Noack R M and Muramatsu A, 2007 *Phys. Rev. Lett.* **98** 210405
[14] Moeckel M and Kehrein S, 2008 *Phys. Rev. Lett.* **100** 175702
[15] Gritsev V, Demler E, Lukin M and Polkovnikov A, 2007 *Phys. Rev. Lett.* **99** 200404
[16] Cazalilla M A, 2006 *Phys. Rev. Lett.* **97** 156403
[17] Rossini D, Silva A, Mussardo G and Santoro G E, 2009 *Phys. Rev. Lett.* **102** 127204
Rossini D, Suzuki S, Mussardo G, Santoro G E and Silva A, 2010 *Phys. Rev.* B **82** 144302
[18] Iglói F and Rieger H, 2011 *Phys. Rev. Lett.* **106** 035701
[19] Calabrese P, Essler F H L and Fagotti M, 2011 *Phys. Rev. Lett.* **106** 227203
[20] Rieger H and Iglói F, 2011 *Phys. Rev.* B **84** 165117
[21] Calabrese P and Cardy J, 2006 *Phys. Rev. Lett.* **96** 136801
Calabrese P and Cardy J, 2007 *J. Stat. Mech.* P06008
[22] Sotiriadis S and Cardy J, 2008 *J. Stat. Mech.* P11003
Sotiriadis S and Cardy J, 2010 *Phys. Rev.* B **81** 134305
[23] Gambassi A and Calabrese P, 2010 arXiv:1012.5294
[24] Eisler V and Peschel I, 2007 *J. Stat. Mech.* P06005
[25] Calabrese P and Cardy J, 2007 *J. Stat. Mech.* P10004
[26] Eisler V, Karevski D, Platini T and Peschel I, 2008 *J. Stat. Mech.* P01023
[27] Iglói F, Szatmári Zs and Lin Y-Ch, 2009 *Phys. Rev.* B **80** 024405
[28] Bayat A, Bose S and Sodano P, 2010 *Phys. Rev. Lett.* **105** 187204
[29] Sodano P, Bayat A and Bose S, 2010 *Phys. Rev.* B **81** 100412
[30] Stéphan J-M and Dubail J, 2011 *J. Stat. Mech.* P08019
[31] Silva A, 2008 *Phys. Rev. Lett.* **101** 120603
[32] Pfeuty P, 1970 *Ann. Phys.* **57** 79
[33] Lieb E, Schultz T and Mattis D, 1961 *Ann. Phys.* **16** 407
[34] Yang C N, 1952 *Phys. Rev.* **85** 808
[35] Cardy J, 1984 *Nucl. Phys.* B **240** 514
[36] Cardy J, 1990 *Phys. Rev. Lett.* **65** 1443
[37] Burkhardt T W and Xue T, 1991 *Phys. Rev. Lett.* **66** 895
[38] Fisher M E and De Gennes P-G, 1978 *C. R. Seances Acad. Sci.* B **287** 207
[39] Turban L and Iglói F, 1997 *J. Phys. A: Math. Gen.* **30** L105
[40] Sachdev A and Young A P, 1997 *Phys. Rev. Lett.* **78** 2220
[41] Bariev R Z, 1979 *Zh. Eksp. Teor. Fiz.* **77** 1217
Bariev R Z, 1979 *Sov. Phys. JETP* **50** 613 (translation)
[42] McCoy B M and Perk J H H, 1980 *Phys. Rev. Lett.* **44** 840
[43] Iglói F, Peschel I and Turban L, 1993 *Adv. Phys.* **42** 683